Developmental Biology xxx (2010) xxx–xxx

Contents lists available at ScienceDirect

Developmental Biology

journal homepage: www.elsevier.com/developmentalbiology

A cell-based model of *Nematostella vectensis* gastrulation including bottle cell formation, invagination and zippering

Carlos Tamulonis [a], Marten Postma [a,1], Heather Q. Marlow [b], Craig R. Magie [c], Johann de Jong [a,2], Jaap Kaandorp [a,*]

[a] Section for Computational Science, Universiteit van Amsterdam, Science Park 107, 1098 XG Amsterdam, The Netherlands
[b] Kewalo Marine Laboratory, Pacific Biomedical Research Center, University of Hawaii, Honolulu, HI 96813, USA
[c] Department of Biology, California State University, Fresno, 2555 E. San Ramon Ave., MS SB73, Fresno, CA 93740, USA

ARTICLE INFO

Article history:
Received for publication 7 May 2010
Revised 30 August 2010
Accepted 9 October 2010
Available online xxxx

Keywords:
Nematostella vectensis
Cell-based model
Invagination
Bottle cells
Zippering

ABSTRACT

The gastrulation of *Nematostella vectensis*, the starlet sea anemone, is morphologically simple yet involves many conserved cell behaviors such as apical constriction, invagination, bottle cell formation, cell migration and zippering found during gastrulation in a wide range of more morphologically complex animals.
In this article we study *Nematostella* gastrulation using a combination of morphometrics and computational modeling. Through this analysis we frame gastrulation as a non-trivial problem, in which two distinct cell domains must change shape to match each other geometrically, while maintaining the integrity of the embryo. Using a detailed cell-based model capable of representing arbitrary cell-shapes such as bottle cells, as well as filopodia, localized adhesion and constriction, we are able to simulate gastrulation and associate emergent macroscopic changes in embryo shape to individual cell behaviors.
We have developed a number of testable hypotheses based on the model. First, we hypothesize that the blastomeres need to be stiffer at their apical ends, relative to the rest of the cell perimeter, in order to be able to hold their wedge shape and the dimensions of the blastula, regardless of whether the blastula is sealed or leaky. We also postulate that bottle cells are a consequence of cell strain and low cell–cell adhesion, and can be produced within an epithelium even without apical constriction. Finally, we postulate that apical constriction, filopodia and de-epithelialization are necessary and sufficient for gastrulation based on parameter variation studies.

Introduction

Nematostella vectensis, the starlet sea anemone, is a member of the phylum Cnidaria, which are basal metazoans (jellyfish, sea anemones, sea pens and corals). Over the past decade, *Nematostella* has become an important model organism in the field of evolutionary developmental biology. Its initial success as a model system can in part be attributed to the flexibility of the organism, which can be easily maintained in a laboratory, regularly spawns eggs and sperm and is amenable to molecular techniques commonly used to study gene expression and morphology (Darling et al., 2005). Subsequent gene expression studies and the sequencing of the genome have shown that *Nematostella*, curiously, shares more genes with humans than either *Drosophila melanogaster* or *C. elegans* (Putnam et al., 2007). Much work on *Nematostella* has been dedicated to the genetic regulation of development (Byrum and Martindale, 2004). However, recent studies (Kraus and Technau, 2006; Magie et al., 2007) have focused more on the mechanics and cell biology of development during gastrulation.

Nematostella is diploblastic and its gastrulation involves the internalization of the presumptive endoderm such that a bi-layer gastrula is formed. After fertilization, *Nematostella* eggs undergo 11 cleavage cycles forming a monolayered coeloblastula (Figs. 1 and 2A; Fritzenwanker et al., 2007). The presumptive endoderm caps the animal pole of the embryo and accounts for roughly one fourth of the epithelium, with the presumptive ectoderm accounting for the rest (Magie et al., 2007). Gastrulation begins by the endoderm undergoing a partial epithelial-to-mesenchymal transition (EMT: Shook and Keller, 2003), in which the cells lose their epithelial organization, constrict their apices and become motile, but remain firmly attached at the apex. As a result, bottle cells form and the endoderm begins to invaginate into the blastocoel (Fig. 2B–C, X; Kraus and Technau, 2006; Magie et al., 2007). As invagination progresses, both endodermal and ectodermal cells extend and retract protrusions from their basal surface. The protrusions,

* Corresponding author. Section Computational Science, Faculty of Science, University of Amsterdam, Science Park 904C, 1098 XH Amsterdam, The Netherlands. Fax: +31 20 5257419.
E-mail address: J.A.Kaandorp@uva.nl (J. Kaandorp).
[1] Current Address: Swammerdam Institute for Life Sciences (SILS), Molecular Cytology Group, University of Amsterdam, Science Park 904, 1098 XH Amsterdam, The Netherlands.
[2] Current Address: Bioinformatics and Statistics Division of Molecular Biology, Netherlands Cancer Institute, Plesmanlaan 121, 1066CX Amsterdam, The Netherlands.

0012-1606/$ – see front matter © 2010 Published by Elsevier Inc.
doi:10.1016/j.ydbio.2010.10.017

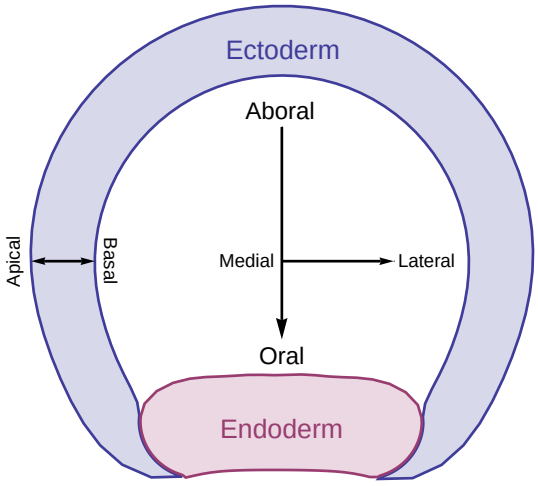

Fig. 1. An "atlas" of the gastrulating *Nematostella* embryo. *Nematostella's* primary axis lies between the oral (=animal) and aboral (=vegetal) poles. The endoderm is centered on the oral pole and consists of approximately 1/4 of the total perimeter of the blastula. The remaining cells compose the ectoderm. The "lateral" direction is defined to be perpendicular to the oral/aboral axis pointing away from the center of the embryo.

resembling filopodia, appear to draw the basal surfaces of the ectoderm and endoderm together by a "zippering" process, resulting in a bi-layered early gastrula (Fig. 2D–F, Y).

Most of the cellular "tools" employed by *Nematostella* embryos are known from other organisms as well. Apical constriction is found in virtually all metazoans and is usually employed as a way of internalizing cells into the embryo, either by invagination or ingression (Keller et al., 2003). Invagination is found in many cnidarians (Byrum and Martindale, 2004; Marlow and Martindale, 2007), the sea urchin (primary invagination: Davidson et al., 1995), the fruit fly (ventral furrow formation: Martin et al., 2008) as well as in many other systems (reviewed in Keller et al., 2003). Bottle cells are found in many systems, for example in *Xenopus* (Hardin and Keller, 1988) and the sea urchin (Kimberly and Hardin, 1998). The zippering process is a feature of epithelial cell adhesion in mammalian cells (Vasioukhin et al., 2000), *D. melanogaster* dorsal closure (Jacinto et al., 2000), epithelial wound healing (Martin and Parkhurst, 2004) and optic cup formation (Chauhan et al., 2009).

In this article, we attempt to associate transformations of the endoderm and ectoderm with the transformations occurring at the cellular level. For this purpose we have developed a cell-based model with novel features. Cell-based models, in which cells are represented

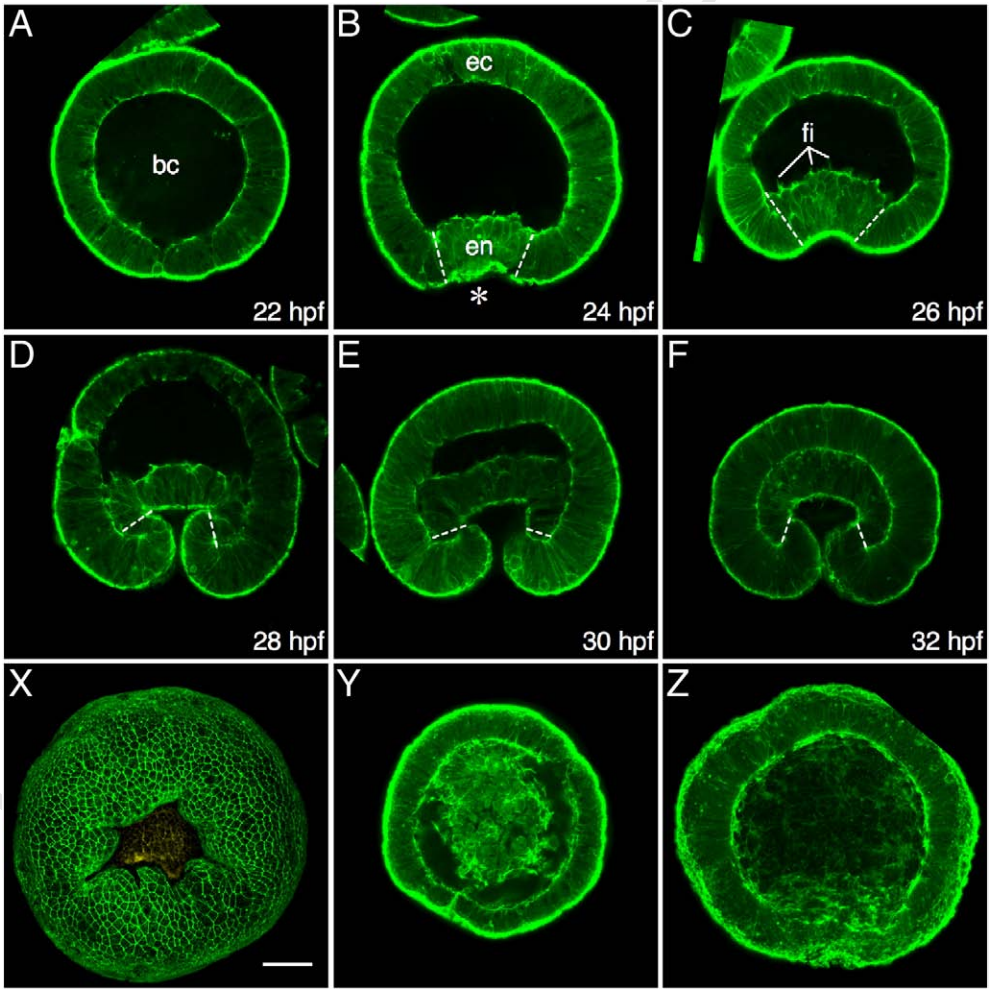

Fig. 2. *Nematostella vectensis* gastrulation. Embryos stained with phalloidin, which marks F-actin and reveals the cytoskeleton of each cell. Images are single optical slices obtained with a scanning confocal microscope. Embryos are oriented such that the oral–aboral axis is vertical with the oral pole at the bottom. Tile height is 250 μm, unless otherwise specified. Legend: (bc) blastocoel; (*) blastopore and oral pole; (···) endo/ectoderm boundary; (en) endoderm; (ec) ectoderm; (fi) filopodia. (A) Just before gastrulation begins the embryo is a spherical coeloblastula. (B) Gastrulation begins with down-regulation of adhesion and apical constriction in the endoderm (C) Apical constriction is followed by invagination and bottle cell formation (D–F) Using filopodia, the endoderm and ectoderm zip up forming a two layer gastrula with a characteristic "mushroom shape" in which the archenteron is laterally stretched. (X–Z) Z-projections of confocal stacks of early gastrulae at different angles. (X) Oral view showing apical side of the invaginating endodermal plate (false colored yellow) and surrounding ectoderm. Scale bar 50 μm. (Y) Aboral view showing basal side of the invaginating endoderm. Endoderm/ectoderm zippering has commenced on one side of the embryo. (Z) Lateral view. Endoderm located at the bottom.

Please cite this article as: Tamulonis, C., et al., A cell-based model of *Nematostella vectensis* gastrulation including bottle cell formation, invagination and zippering, Dev. Biol. (2010), doi:10.1016/j.ydbio.2010.10.017

as individuals, have become increasingly popular as a means to model biological systems with greater detail (Davidson et al., 2010). The simplest type assumes cells are spherical or ellipsoidal such that each cell can be represented as a single point—the center of the sphere or ellipsoid. These models have been used to study cell sorting, tissue rheology and collective cell movement (Palsson and Othmer, 2000) as well as cell spreading and proliferation (e.g. Drasdo and Höhme, 2005). Vertex models represent the cell boundary explicitly as a set of vertices. However these models are still limited to simple polygonal cell shapes and cells must form a continuous sheet from which the cells cannot detach. These models have been used to model cell rearrangements during tissue stretching (Chen and Brodland, 2000) and cell intercalation (e.g. Rauzi et al., 2008), embryonic polarity determination (Honda et al., 2008), gastrulation by epiboly (Weliky and Oster, 1990) and gastrulation by invagination (e.g. Davidson et al., 1995; Odell et al., 1981; Pouille and Farge, 2008). Finally, simple yet powerful models based on the Cellular Potts Model (CPM) formalism (Graner and Glazier, 1992) have gained widespread use, including in developmental biology (Marée and Hogeweg, 2001). CPM models allow for arbitrary cell shapes and were originally used for modeling cell sorting phenomena, but have been adapted over the years to include numerous other phenomena. These models are attractive due to their simplicity, but unfortunately they are less suitable for modeling rigid constraints, such as fixed adhesion complexes, or for systems in which the cells exert forces with non-local effects, such as apical constriction.

Given the relative simplicity of the embryonic geometry and the gastrulation process in *Nematostella*, we found that this system offers a unique opportunity to create a single computational model that integrates all the various known cell behaviors that shape the *Nematostella* mono-layered blastula into a bi-layered gastrula. We have developed a cell-based model with novel features based on the pioneering work of Odell et al. (1981, 2004). The model is capable of representing arbitrary cell shapes and places no restriction on cell neighbors or cell movement. We found that the model allows us to capture *Nematostella* gastrulation in detail and test whether the processes reported in the literature are plausible and sufficient for gastrulation. We also investigated the mechanical stability of the blastula and the mechanics bottle cell formation.

Materials and methods

Embryo preparation

Embryo fixation, staining and imaging

Nematostella vectensis adults were spawned using light and temperature cues and fertilized eggs were dejellied as previously reported (Fritzenwanker et al., 2002). Embryos were raised to the desired developmental stage and then fixed, stained with propridium iodide and phalloidin and cleared as reported by Magie et al. (2007). Confocal stacks were collected on a Zeiss LSM510 confocal microscope (Carl Zeiss, Jena, Germany).

Blastocoel injections of dextran

Embryos were cultured to the mid-blastula stage when a coeloblastula is clearly visible, prior to the onset of gastrulation. The blastocoel was injected with FluoroRuby Dextran (50 mg/ml in KCl) and embryos were then reared to through gastrulation and fixed, stained and imaged as above.

Morphometrics

Images were first processed using ImageJ (V1.41o) to semi-automatically normalize the scale and the embryo rotation, crop and finally manually trace the endoderm and ectoderm domains (as polygons) of each embryo. The endoderm/ectoderm boundary is very distinct in early gastrulae. The endoderm appears as a disorganized mass of apically bound cells whereas the ectoderm appears as an organized epithelium. Geometrical data were then exported to Mathematica (v7.0.1) for further treatment. Relative invagination depth was calculated as the ratio of the distance between the oral and aboral poles and the diameter of the embryo. Volume/surface area of a domain was estimated by calculating volume/area of the solid/surface of revolution of the traced polygon/polyline around a horizontal axis passing through the centroid of the polygon under consideration. Average thickness of a domain was calculated by automatically taking evenly spaced samples perpendicular to the longitudinal axis of the domain.

The model

Model geometry

To be able to incorporate all the cell behaviors known to occur in *Nematostella* gastrulation, we designed a model that offers a detailed boundary description of the cells, allowing these to take on any shape and to be differentiated along their apical–basal axis. Each cell is represented by an 84 vertex polygon that is initially wedge shaped (Fig. 3A). The model blastula used is 200 μm in diameter, the blastoderm is 32 μm thick and is composed of 87 identical wedge cells, based on the available morphological data of the late blastula (Kraus and Technau, 2006; Magie et al., 2007) (Fig. 3B).

The cells are divided into two populations: cells 1–24 are endodermal cells while cells 25–87 are ectodermal (this ratio is based on domain morphology and in-situ hybridization staining of endoderm genetic markers such as NvSnail, see Magie et al., 2007). Each cell is also split into two parts: vertices 1–75 (edges 1–75 and 84) constitute the basal–lateral portion of the cell boundary, whereas vertices 76–84 (edges 76–83) constitute the apical portion of the cell. As described below, the endodermal and ectodermal cells will have different properties and each cell will also be differentiated apico-basally. See Table 1 for a summary of the model parameters and their default values.

Dynamics

The dynamics of the model are driven by simple Newtonian mechanics and the position of each vertex, $\mathbf{r}_{c,i}$, is governed by the equation:

$$m_{c,i}\frac{d^2\mathbf{r}_{c,i}}{dt^2} = \mathbf{F}_{c,i} - \eta_{c,i}\frac{d\mathbf{r}_{c,i}}{dt} \quad c = 1, \ldots, 87 \quad v = 1, \ldots, 84$$

where $\mathbf{F}_{c,i}$ is the total force acting on the vertex, $m_{c,i}$ and $\eta_{c,i}$ are the mass and the damping parameter of the vertex, which controls the viscosity of the vertex's movement during simulations. For all vertices we take $m_{c,i}=1$ and $\eta_{c,i}=0.1$.

All the processes in the model are described in terms of vector forces. Running a simulation step consists of determining the forces acting on each vertex and solving the resulting system of differential equations using the Velocity Verlet numerical integration method with timestep $\Delta t=0.1$.

Forces

Springs. Each edge of every cell is loaded with a spring that controls its length by exerting a restorative force proportional to the strain:

$$F = k\ (l - l_0)l_0$$

where k is the spring stiffness, l is the edge length and l_0 is the spring's rest length. The rest length is parameterized by s such that $l_0=(1-s)$ L_0 where $0\le s<1$ is called the "strain factor" and L_0 is the initial length of the edge.

Every vertex is connected to each of its two neighbors by a spring (Fig. 3B–C). These springs have different parameters depending on

Please cite this article as: Tamulonis, C., et al., A cell-based model of *Nematostella vectensis* gastrulation including bottle cell formation, invagination and zippering, Dev. Biol. (2010), doi:10.1016/j.ydbio.2010.10.017

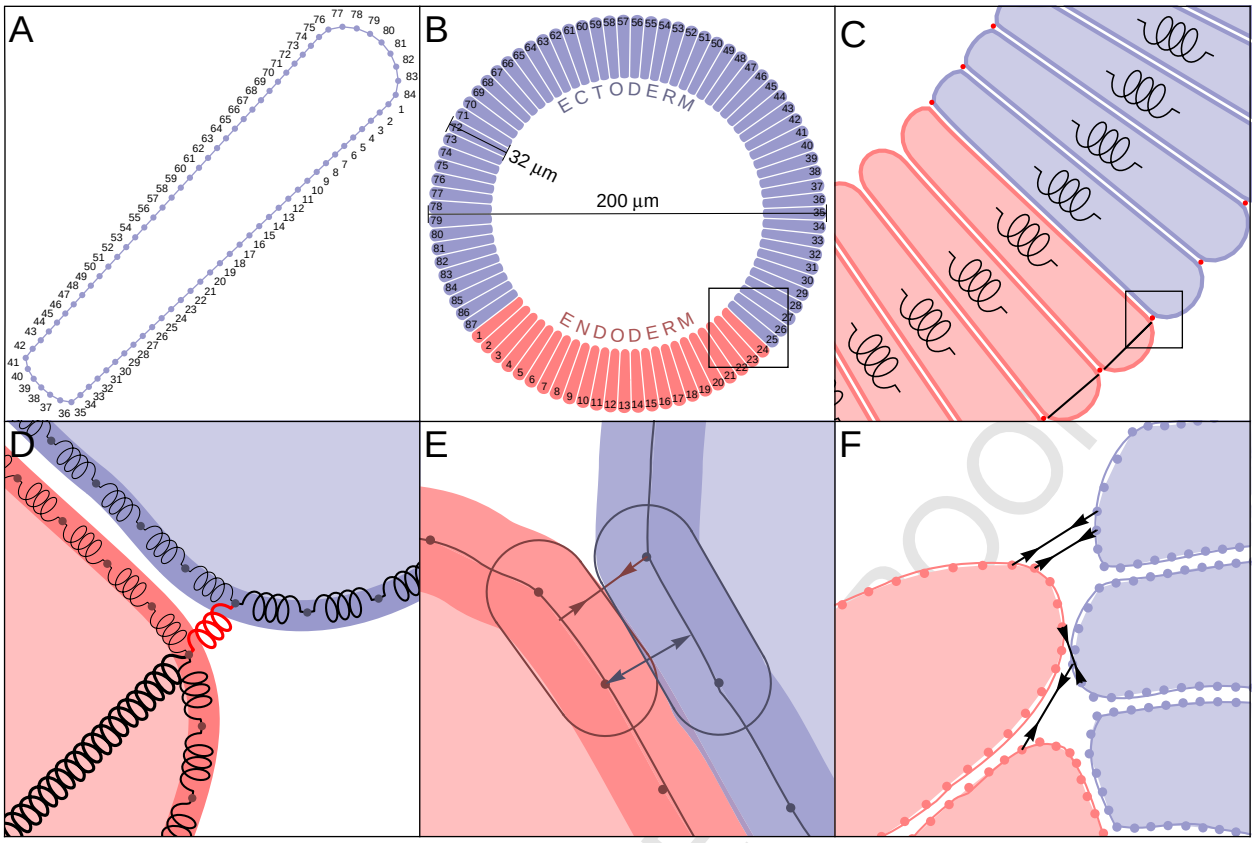

Fig. 3. Model architecture. (A) Each cell is modeled as a complex polygon with 84 vertices. Initially every cell is wedge shaped. Vertices 76–84 are considered the apical part of the cell and the remainder is the basal/lateral part. (B) The blastula is composed of a ring of 87 identically shaped wedge cells split into two functionally distinct domains: the endoderm (red) and the ectoderm (blue). (C) Each cell has a stiffly elastic cytoplasm. All the cells are connected apically by stiff springs and the ectodermal cells are also connected basally (red dots). Endodermal cells have a spring across their apical diameter to mimic an actin–myosin belt. (black line) (D) The cell cortex is modeled as a set springs connected in series. All cells are joined apically by a very stiff spring (red spring) and the endodermal cells have a highly contractile apical belt (thick spring). The outer apical springs are stiffer than the rest to provide mechanical support to the blastula (medium springs). (E) Contact between cells is modeled as an elastic force between edges and vertices. The red edge is attracting a blue vertex to its surface through adhesion (red arrows); whereas the blue edge is repulsing a slightly overlapping red vertex (blue arrows). (F) Filopodia form stochastically between uncovered vertices of the endoderm and ectoderm. Each filopodium exerts a constant attractive force for a fixed period of time.

whether they are in the apical or basal portion of the cell boundary. Basal/lateral springs have $k=1$ and $s=0.375$. Apical springs also have $s=0.375$ but are stiffer with $k=10$.

Table 1
Model parameters. The table summarizes the principal model parameters. Parameters are set to the values specified in the table unless otherwise specified in the text.

Integration	Timestep, Δt		0.1
	Viscosity, η		1
Embryo	Diameter		200 μm
	Thickness		32 μm
	Num. of cells	Ectoderm	63
		Endoderm	24
Springs	Stiffness, k	Apical	5
		Baso-lateral	1
		Belt	100
		Junctions	100
	Strain factor, s	Apical	0.375
		Baso-lateral	0.375
		Belt	0.65
		Junctions	0
Cytoplasm	Stiffness, k_A		10
Adhesion	Range, a		0.5 μm
	Intensity, α	Endo–Endo	0
		Endo–Ecto	2
		Ecto–Ecto	2
Filopodia	Period, T_1		20
	Range, ρ		10 μm
	Force, f		0.3
	Duration, T_2		200

The cells are linked to their neighbors on either side by an intercellular spring that connects the apical corners of the cells (between vertices $\langle c, 76\rangle$ and $\langle c+1, 84\rangle$, $c=1, \ldots, 87$). In some simulations the ectodermal cells are also bound by springs at their basal corners, to simulate a tightly bound epithelium (between vertices $\langle c, 41\rangle$ and $\langle c+1, 35\rangle$ $c=25, \ldots, 86$; Fig. 3B–C). These "junction" springs are initially at rest ($s=1$) and are very stiff ($k=100$).

Actin–myosin contractile rings are thought to be the basis of apical constriction in *Nematostella* (Kraus and Technau, 2006; Magie et al., 2007), which occurs in the endoderm at the onset of gastrulation. To simulate apical contractile rings in 2D, an intra-cellular spring is placed between each endodermal cell's apical corners (between vertices $\langle c, 76\rangle$ and $\langle c, 84\rangle$, $c=1, \ldots, 24$; Fig. 3C). The ring strain factor is set to $s=0.65$ and the stiffness to $k=100$.

Cytosol. We assume that the cytoplasm is also linearly elastic, so that the pressure on the cell boundary is proportional to the difference between the current area (A) and the initial area of the cell (A_0) times the cytoplasm stiffness ($k_A=10$):

$$E_A = \frac{1}{2} k_A \left(\frac{A-A_0}{A_0}\right)^2$$

The area of a cell is given by the standard formula for the area of a polygon:

$$A = -\frac{1}{2}\sum_{i=1}^{84} x_i y_{i+1} - x_{i+1} y_i.$$

Please cite this article as: Tamulonis, C., et al., A cell-based model of *Nematostella vectensis* gastrulation including bottle cell formation, invagination and zippering, Dev. Biol. (2010), doi:10.1016/j.ydbio.2010.10.017

The area energy is translated into vertex forces by taking the gradient of the energy at each vertex:

$$F_i = -\nabla_i\left[\frac{1}{2}k_A\left(\frac{A-A_0}{A_0}\right)^2\right] = -k_A\frac{A-A_0}{A_0}\langle y_{i-1}-y_{i+1}, x_{i+1}-x_{i-1}\rangle.$$

Contact. Contact forces are defined between edge–vertex pairs. The edges are "capsule" shaped with flat sides and semi-circular caps (Fig. 3E). Any vertex that enters an edge's exclusive area is repelled from the capsule. Vertices may also be attracted to the capsule perimeter if they move away from the edge and the edge and vertex are adherent. The repulsion/adhesion force intensity is given by:

$$F = \begin{cases} -R(d-h)/h & 0 \le d \le h \\ -\alpha\left(1-\frac{2}{a}\left|d-\left(h+\frac{a}{2}\right)\right|\right) & h < d \le a+h \end{cases}$$

where:

- d is the length of the displacement vector between the edge and the vertex
- $h = 0.75$ is the capsule diameter
- $a + h = 1.25$ is the diameter of the capsule's adhesive area
- $\alpha = 2$ is the adhesion strength and
- $R = 10$ is the repulsion strength.

The direction of the force is along the direction of the displacement vector, which is the shortest vector connecting the edge to the vertex. The displacement vector d between an edge $\mathbf{e} = \mathbf{r}_j - \mathbf{r}_i$, and a vertex $\mathbf{r}_k$ is given by:

$$\mathbf{d}(\mathbf{r}_i, \mathbf{r}_j, \mathbf{r}_k) = \begin{cases} \mathbf{r}_k - \mathbf{r}_i & u \le 0 \\ \hat{\mathbf{e}} \times (\mathbf{r}_k - \mathbf{r}_i) \times \hat{\mathbf{e}} & 0 < u < 1 \\ \mathbf{r}_k - \mathbf{r}_j & u \ge 1 \end{cases}$$

where:

- $\hat{\mathbf{e}} = \mathbf{e}/\|\mathbf{e}\|$ is the normalized edge vector and
- $u = \frac{(\mathbf{r}_k - \mathbf{r}_i)\cdot\mathbf{e}}{\mathbf{e}\cdot\mathbf{e}}$ is the normalized projection of the vertex onto the edge.

If $u \le 0 / u \ge 1$, then the intruding vertex $\mathbf{r}_k$ is touching one of the capsule's rounded ends and is only interacting with one of the edge's vertices. If $0 < u < 1$, then the intruding vertex is touching one of the capsule's sides and is therefore interacting with both edge vertices simultaneously. In this case the interaction force is split between the vertices such that the torque around the contact point is zero and the sum of all forces is also zero:

	$\mathbf{F}_k$	$\mathbf{F}_i$	$\mathbf{F}_j$
$u \le 0$	$F\hat{\mathbf{d}}$	$-F\hat{\mathbf{d}}$	0
$0 < u < 1$	$F\hat{\mathbf{d}}$	$-(1-u)F\hat{\mathbf{d}}$	$-uF\hat{\mathbf{d}}$
$u \ge 1$	$F\hat{\mathbf{d}}$	0	$-F\hat{\mathbf{d}}$

Filopodia. Finally, filopodia offer a long-range adhesive mechanism that can bridge the gap between the endoderm and ectoderm and force the two layers to fit. We model filopodia extension and adhesion as a stochastic process in which each cell pulls on other cells within a given range (Fig. 3F).

Filopodia form stochastically between adhesive vertices. On average, one filopodium forms every $T_1 = 20$ s per endodermal cell. When a filopodium is initiated, first a random suitable vertex is selected from the endodermal cell and then all vertices within a radius $\rho = 10\,\mu$m are found and again another suitable random vertex is selected from these. The vertices are suitable if both vertices are adhesive and neither is covered by an adjoining polygon. Once a filopodium is formed, the vertices feel a constant force $f = 0.3$ that pulls them together for $T_2 = 20$ s after which they are released.

Results

Morphometrics

We analyzed 47 confocal sections of *Nematostella* embryos between the blastula and the early gastrula stages, ~22–32 hours post-fertilization (hpf) at 16 °C. The embryos were first sorted by relative invagination depth (see Materials and methods) and then partitioned these into six bins corresponding to 22, 24, 26, 28, 30, 32 hpf assuming a roughly linear relationship between normalized invagination depth and time. We then measured various morphological metrics of each embryo and calculated the mean and standard error of the mean (SEM) of each bin. We also performed Student's *t*-tests between the bins to test for significant differences.

The diameter and total volume of the embryos (blastoderm and blastocoel fluid) decrease by a significant amount during gastrulation, although a significant change in the blastoderm volume was not detected (Fig. 4A–B). This indicates that there may be little to no retention of the blastocoel fluid by the cells and that the bulk of it is somehow removed from the embryo as gastrulation progresses. Within the blastoderm a significant increase in the volume of the endoderm was detected, however we could not determine whether this came at the expense of the ectoderm or whether the endoderm retains the blastocoel fluid, as the endoderm volume gain is well within the measurement error of the ectoderm volume (Fig. 4C).

Morphologically, gastrulation begins by a decrease of the apical diameter of the endodermal cells at around 22 hpf. By measuring and comparing the cell diameters of constricted and unconstricted cells in oral views of embryos, ($N = 5$, Fig. 2X) we estimated that the endodermal cells' apical diameter is reduced by 50–65%, comparable with apical constriction in *Drosophila* ventral furrow formation (Martin et al., 2008). A decrease in the apical surface area of the endoderm was also detected (Fig. 4D). Unlike *Drosophila*, however, the cells appear to use a postulated actin–myosin purse-string, instead of a contracting apical mesh, since the apical surface of the constricting cells bulges, maintaining its surface area even as the apical diameter of the cells decreases (Kraus and Technau, 2006; Magie et al., 2007).

Measurement of the basal surface area of the endoderm and ectoderm revealed that prior to gastrulation the basal ectoderm surface area is much larger than the basal endoderm surface area (Fig. 4E). During the course of gastrulation, however, the basal surfaces of the ectoderm and endoderm decrease and increase, respectively, and eventually equalize as the two surfaces come into apposition.

Apical constriction induces a sharp increase in the thickness (apico-basal dimension) of the endoderm, which then either passively relaxes or actively contracts to less than its initial thickness by the end of zippering (Fig. 4F). As it thins, the endoderm also increases its breadth two-fold (Fig. 4G) and increases its volume by about 75% (Fig. 4C).

In contrast to the endoderm, no significant changes in volume or breadth were detected for the ectoderm (Fig. 4C, G), however its thickness does vary differentially in time and space. Shortly after gastrulation begins, the ectoderm thins, followed by a phase in which the ectoderm thickens differentially starting at the oral end of the ectoderm, with the "thickening front" moving towards the aboral pole (Fig. 4H). On average, the early gastrula ectoderm is thicker than the blastula stage. The ectoderm becomes thickest at the blastopore margin where it bends inwards into the blastocoel and thins towards the aboral pole and the ecto/endoderm boundary, where it tapers abruptly. Both the thickened and tapered regions of the oral ectoderm

Please cite this article as: Tamulonis, C., et al., A cell-based model of *Nematostella vectensis* gastrulation including bottle cell formation, invagination and zippering, Dev. Biol. (2010), doi:10.1016/j.ydbio.2010.10.017

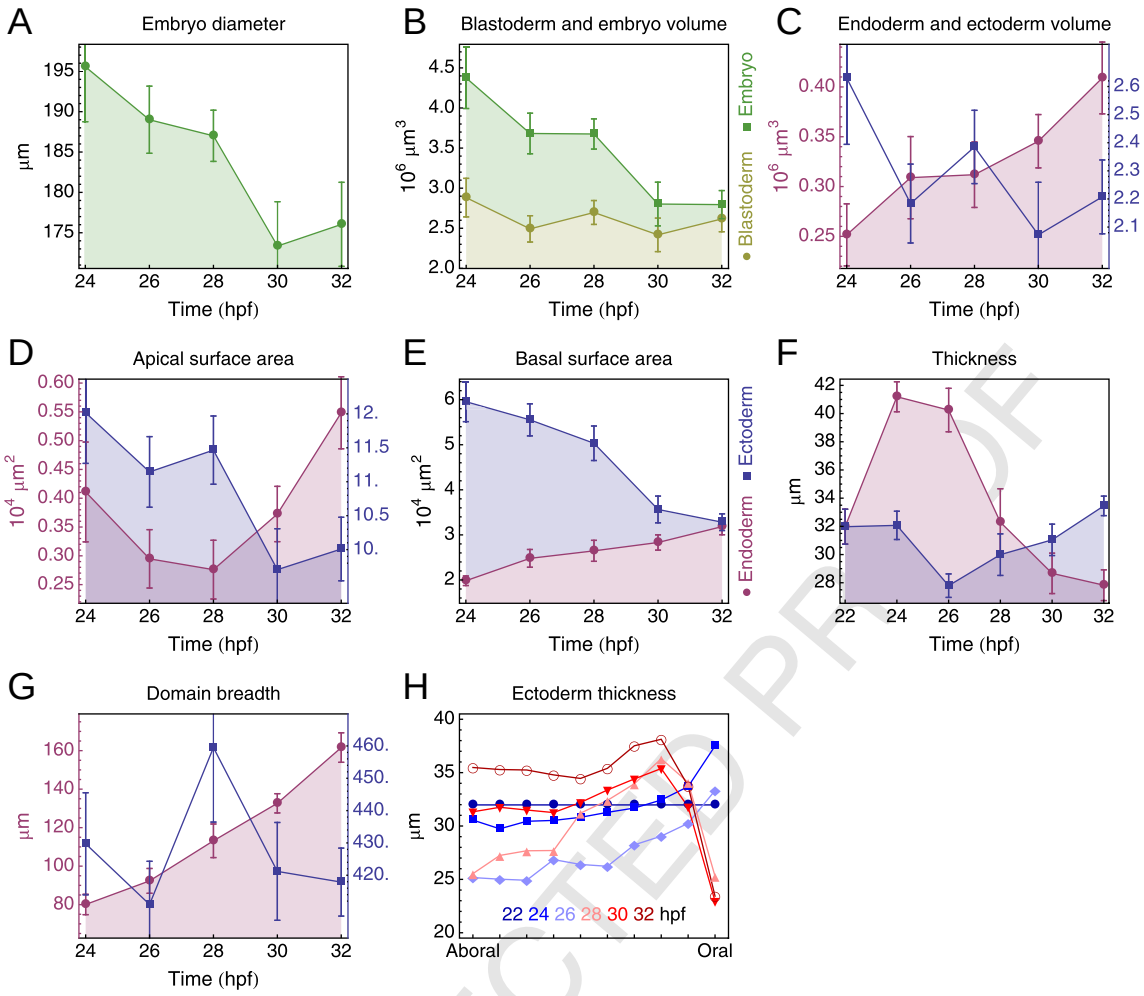

Fig. 4. Morphometrics of *Nematostella* gastrulation. Error bars represent the standard error of the mean (SEM). Endoderm data are in red and the ectoderm in blue unless otherwise labeled. (A) Embryo diameter. The embryo diameter decreases significantly during gastrulation. (B) Blastoderm and embryo volume. The total embryo volume decreases markedly during gastrulation (blue), whereas the blastoderm volume does not change significantly. This indicates that the blastocoel fluid is removed from the embryo during gastrulation. (C) Endoderm volume as a fraction of the blastoderm volume. The endoderm volume increases significantly during gastrulation. (D) Apical surface area. The endoderm's apical surface area shrinks and then recovers (left axis), whereas in the ectoderm it shrinks significantly (right axis). (E) Basal surface area. Initially the basal surface of the ectoderm is much larger than that of the endoderm, although the two eventually converge. (F) Thickness. The endoderm thickens sharply during apical constriction and gradually contracts during gastrulation (left axis). Conversely, the ectoderm thins somewhat initially and then gradually thickens (right axis). (G) Breadth. The breadth of the endoderm increases nearly two-fold during gastrulation as the endodermal cells increase in volume and spread onto the ectoderm. No significant changes in the ectoderm breadth were found. (H) Spatio-temporal ectoderm thickness. The maximum thickness is at the blastopore lip where the ectoderm bends inwards and minimum at the aboral pole. The gradient towards the aboral pole is steeper at the beginning of gastrulation, but gradually flattens.

are maintained during gastrulation, however the gradient of thickness towards the aboral pole eventually flattens.

Summarizing, during *Nematostella* gastrulation, the endodermal and ectodermal geometries are not static, but are actively shaped allowing the two layers to be joined. As we explore in the next sections, simple mechanical processes can account for many of these shape changes.

Mechanical equilibrium of the blastula requires stiffened cell apices

Before we begin the simulations, it is desirable that we set the model parameters such that the embryo is in mechanical equilibrium. Each cell's target area is set to its initial area and the area stiffness is set such that the cell area varies less than 5%. One must then define the target spring lengths (l_0) and stiffness parameters (k), which we also refer to as the contractility of the cell. As a base value, we set all $k=1$. A trivial solution for equilibrium would then be to set the spring rest lengths to their initial length $l_0 = L_0$. As the target cell area is also equal to each cell's initial area, the system would be in equilibrium as there would be no strain. However, cells are contractile (Lecuit and Lenne, 2007) and tend to round up when suspended (Garnett, 1980). To simulate this behavior, we set the rest lengths of the springs to a fraction of their initial length $l_0 = (1-s)L_0$, with $0 \le s < 1$, where we call s the strain factor. For our simulations we used $s = 0.375$, which was calculated so that the springs are relaxed if the cell is perfectly round.

In the context of the *Nematostella* blastula and its wedge shaped cells, contractility produces radial forces along the lateral perimeter of the cells, and also circumferential forces along their apical perimeter. The contractile radial forces tend to thin the cell layer, which, assuming the cell volumes are constant, must increase the diameter and the circumference of the embryo. In contrast, the circumferential forces will tend to contract the circumference, decrease the diameter and increase the thickness of the cell layer. The two competing forces meet at the cell corners, where they are almost perpendicular and are thus weakly coupled. If we assume the cell is homogenously contractile, then the radial component of the circumferential force will be too weak to cancel the expansive radial force (Fig. 5A–B). An additional radial force resisting embryo expansion must be supplied.

Please cite this article as: Tamulonis, C., et al., A cell-based model of *Nematostella vectensis* gastrulation including bottle cell formation, invagination and zippering, Dev. Biol. (2010), doi:10.1016/j.ydbio.2010.10.017

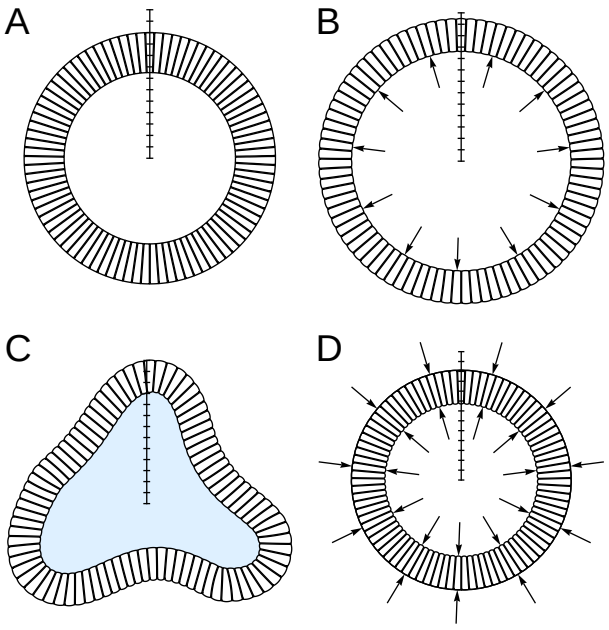

Fig. 5. Blastomere apices must be stiffer to constrain embryo dimensions. Figures correspond to simulation steady states. (A) The initial geometry of the embryo. We want to choose the mechanical parameters such that the embryo is initially in equilibrium. (B) Assuming homogenous intra-cellular contractility results in the embryo expanding its diameter, as the radial contractile force is only weakly resisted by the circumferential contractile force. (C) Assuming the blastocoel is sealed puts pressure on the embryo to keep its dimensions. This equilibrium is unstable, however, and soon the embryo loses its shape as its surface area increases. (D) Setting the cell apices to be 10× more contractile than their baso-lateral sides is sufficient for the embryo to maintain its dimensions and implicitly conserves embryo volume.

Nematostella embryos do not possess a stiff outer matrix, such as the hyaline layer in sea urchin embryos, which could provide mechanical resistance to embryo expansion. A simple hypothesis would be that the cells are not homogenously contractile, but are more contractile at their apical ends. This is consistent with the observation that F-actin is highly localized at the apical ends of all cells (Fig. 2 and Magie et al., 2007). *Nematostella* blastomeres also have an F-actin enriched ring around their apical perimeter forming an outer mesh around the embryo reminiscent of chicken wire (Fig. 2X). This mesh could also passively resist the expansion of the embryo due to cellular contractility.

Another important factor to consider is the blastocoel. It is unclear whether it is sealed off from the environment, or whether fluid may flow freely in and out. Sea urchin embryos, for example, lose less than 2% of their volume when compressed (Davidson et al., 1999). If the *Nematostella* blastula is also effectively sealed, then the blastocoel volume must remain constant. In that case, any force applied to the blastula that entails a change in the blastocoel volume, such as cell contractility causing an expansion of the embryo, would be canceled by internal hydrostatic pressure.

We have experimented with all three hypotheses and found that the apical springs of the cells need to be approximately 10 times stiffer than their baso-lateral springs in order for the embryo to be in quasi-equilibrium when simulations begin (i.e. embryo dimensions do not change, although the cell ends do round slightly, Fig. 5D). The increased apical stiffness compresses the cells against each other like the wedges in an arch and resists the cells' tendency to round up, which would result in the embryo expanding in diameter. The apical stiffness may be divided between the apical perimeter of the cell or the contractile ring in any combination $k_{ap} + k_{ring} = 10$, however in order for the cells apices to remain flat, as they appear to be in actual embryos, we find that the $k_{ap} \geq 5$, otherwise the squeezing apical belts make the apical surfaces bulge.

We found that these conditions are necessary regardless of whether or not we include blastocoel pressure in the model. If we constrain the blastocoel such that its volume remains practically constant (in the same manner we constrain each cell's volume), and the combined apical stiffness of the cells is insufficient, then the embryo becomes unstable and eventually loses its circular shape as the outer surface of the embryo expands, becoming irregularly shaped instead (Fig. 5C).

We conclude that in order for the *Nematostella* blastula to be in mechanical equilibrium the cells' apical ends must be stiffer than the rest of the cell in order to resist the contractility forces parallel to the cell–cell interface, which will tend to expand the blastoderm surface area. This is consistent with findings in the sea urchin embryo, where the apical ECM was found to be responsible for the bulk of the embryo's stiffness (Davidson et al., 1999). Surprisingly, the sea urchin embryo shrinks, rather than expands, when the ECM is disrupted, although the reason for this is unknown.

Bottle cells are a consequence of cell contractility, low cell–cell adhesion and mechanical constraint

In the previous section we assumed that the cells are all tightly adherent to simulate the late *Nematostella* blastula, in which the cells form a monolayered epithelium. The beginning of gastrulation is marked by the partial de-epithelialization of the pre-endodermal cells at animal pole of the blastula, during which the cells reduce the number of cell–cell adhesion complexes between them and appear to loosen. The cells all retain their apical, belt-like, zonula adherens junction however, maintaining the integrity of the monolayer. When we reduce cell–cell adhesion in the virtual embryo, we observe that the cells lose their regular epithelial organization and assume a configuration in which every odd cell bulges over its two squatting neighbors (Fig. 6A). The bulging cells are very reminiscent of bottle cells, commonly associated with epithelial-to-mesenchymal transitions and apical constriction (Fig. 2B–C).

We found that bottle cell formation is a function of three parameters: the strain factor, cell–cell adhesion and contractility. By reducing the cortical strain factor we find that the bottle cells bulge less (Fig. 6B) and if we also increase cell–cell adhesion and/or decrease contractility the cells remain columnar (Fig. 6C). Therefore we find that cell contractility drives bottle cell formation, whereas cell–cell adhesion acts as an impediment to this process.

We hypothesize that an epithelium will spontaneously reorganize into a bottle cell configuration if three conditions are met: (a) the cells

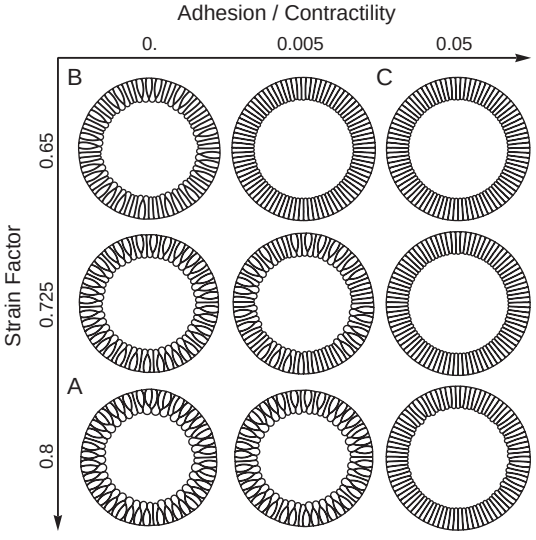

Fig. 6. Bottle cell formation as a function of the cortex strain and the ratio of adhesion strength to contractility.

Please cite this article as: Tamulonis, C., et al., A cell-based model of *Nematostella vectensis* gastrulation including bottle cell formation, invagination and zippering, Dev. Biol. (2010), doi:10.1016/j.ydbio.2010.10.017

are constrained laterally, (b) cell–cell adhesion is low and (c) the cells are under sufficient strain. We also find that this configuration is a natural consequence of mechanics, as it reflects a local minimum in the energy landscape of the system, and need not be regulated by a complex cellular program that dictates the specific cell shapes and cellular organization.

Invagination, filopodia and reduced cell–cell adhesion are necessary, and when combined, sufficient, for Nematostella gastrulation

Gastrulation in real embryos begins with the partial-EMT of the presumptive endoderm, which involves the down-regulation of adhesion and apical constriction. We set endodermal cell–cell adhesion to zero ($\alpha_{en-en}=0$) and the belt strain factor to $s=0.65$, the highest value found during measurements (i.e. apical cell diameters were found to shrink up to 65%, see Morphometrics). We then start the simulations (Movie 1) and gradually increase the contractility of the belts until the target length is reached (Fig. 7A–B).

We observe that constriction makes the apical ends of the cells bulge slightly, but the bulk of the cell cytoplasm is forced towards the basal end. The cells cannot expand laterally due to the neighboring ectoderm, so the cells expand in the apical–basal direction, thickening the layer. Initially, all the cells elongate uniformly along their apico-basal axis. However we also assumed that the endodermal cells do not adhere to each other and so, as constriction progresses, the domain loses its organized structure and the cells assume a bottle cell configuration (Fig. 7B). The bottle cells are strained along their apico-basal axis and the resulting force buckles the endoderm inwards producing an invagination.

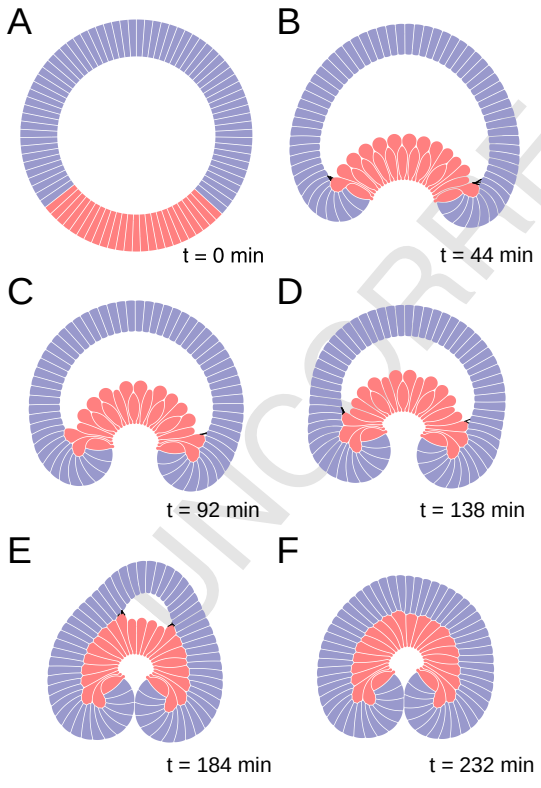

Fig. 7. Model results. *t* refers to simulation time. (A) The initial blastula geometry consists of 87 identical wedge shaped cells organized in a ring. (red cells) endoderm; (blue cells) ectoderm. (B) Gastrulation begins by shortening the apical diameter of the endodermal cells by 65%. The cells initially elongate apico-basally and then organize into an alternating bottle/squat cell configuration. (C) The endodermal plate buckles inwards as the elongated cells contract. (D–F) Filopodia, which form stochastically between the basal endoderm and ectoderm, "zipper" the two layers together.

As the endoderm invaginates, the basal endoderm and ectoderm surfaces are placed at a less obtuse angle (Fig. 7C). This brings the opposing basal endoderm and ectoderm vertices into range, allowing filopodia to attach, which in turn draw the two layers closer (Fig. 7C–E). The lateral most cells of the endodermal plate are the first to attach to the ectoderm. These cells act as stretched springs and pull the endodermal plate laterally such that the second most lateral cells are within filopodial range of the ectoderm. Zippering thus proceeds discretely, as cell by cell the endoderm is joined to the ectoderm. Each cell spreads considerably on the ectoderm, usually covering 2–3 cell diameters, which allows the basal surface area gap between the ectoderm and endoderm to be bridged. Finally, a two-layered gastrula is formed in which the basal endoderm and ectoderm fit together (Fig. 7F) with the characteristic laterally stretched archenteron.

We determine the quality of a gastrulation simulation using the following measures:

(1) the endoderm should come into complete apposition with the ectoderm, closing the blastocoel completely (can be quantified by measuring the blastocoel volume, optimal value would be 0);
(2) the ectoderm basal surface should be entirely covered by the endoderm (can be quantified by the difference between the endoderm and ectoderm basal surface areas, optimal value would be 0);
(3) ideally the archenteron should be stretched laterally, as this better reflects *Nematostella* gastrulae (can be quantified as the ratio between the oral–aboral and lateral dimensions of the archenteron, values <1 are preferable).

Using the chosen parameters (Table 1) we can simulate gastrulation quite well according these criteria (Fig. 7F). The chosen parameters are not finely tuned and can be changed by small amounts without affecting gastrulation quality. However, by further manipulating the main parameters of each process we observe a gradual decay in the quality of gastrulation as follows (Fig. 8):

(a) Reducing the force exerted by filopodia handicaps zippering and causes gaps to appear between the endoderm and ectoderm, especially around the blastopore lip where the blastoderm bends inwards (Fig. 8A–E). Sealing these gaps produces significant lateral tension, which is probably why the archenteron is stretched laterally in *Nematostella* gastrulae. Therefore, invagination alone appears to be insufficient for the ectoderm and endoderm to fit precisely, as the endoderm will only tangentially contact the ectoderm at the poles (Fig. 8E).
(b) The model gastrulates for a wide range of apical constriction parameters, but a minimum amount is still required to produce an invagination that is deep enough for zippering to initiate and allow the endoderm and ectoderm to be brought together (Fig. 8F–J).
(c) Retaining adhesion between endoderm cells reduces the ability of the endoderm cells to fan-out and spread over the ectoderm, causing a mismatch between the basal surfaces of the two layers (Fig. 8K–O).

Based on these results, we suggest that filopodia, apical constriction and down-regulation of endodermal cell–cell adhesion are essential processes in order to complete gastrulation.

Discussion

Bottle cell formation

In *Nematostella*, apico-basal contractility in the endoderm is stimulated by the strain brought on by apical constriction. The cells, constrained laterally by a stiff ectoderm, extend basally as the bulk of their cytoplasm is shifted in this direction. The cells do not all remain extended. Some cells contract their basal end and expand laterally,

Please cite this article as: Tamulonis, C., et al., A cell-based model of *Nematostella vectensis* gastrulation including bottle cell formation, invagination and zippering, Dev. Biol. (2010), doi:10.1016/j.ydbio.2010.10.017

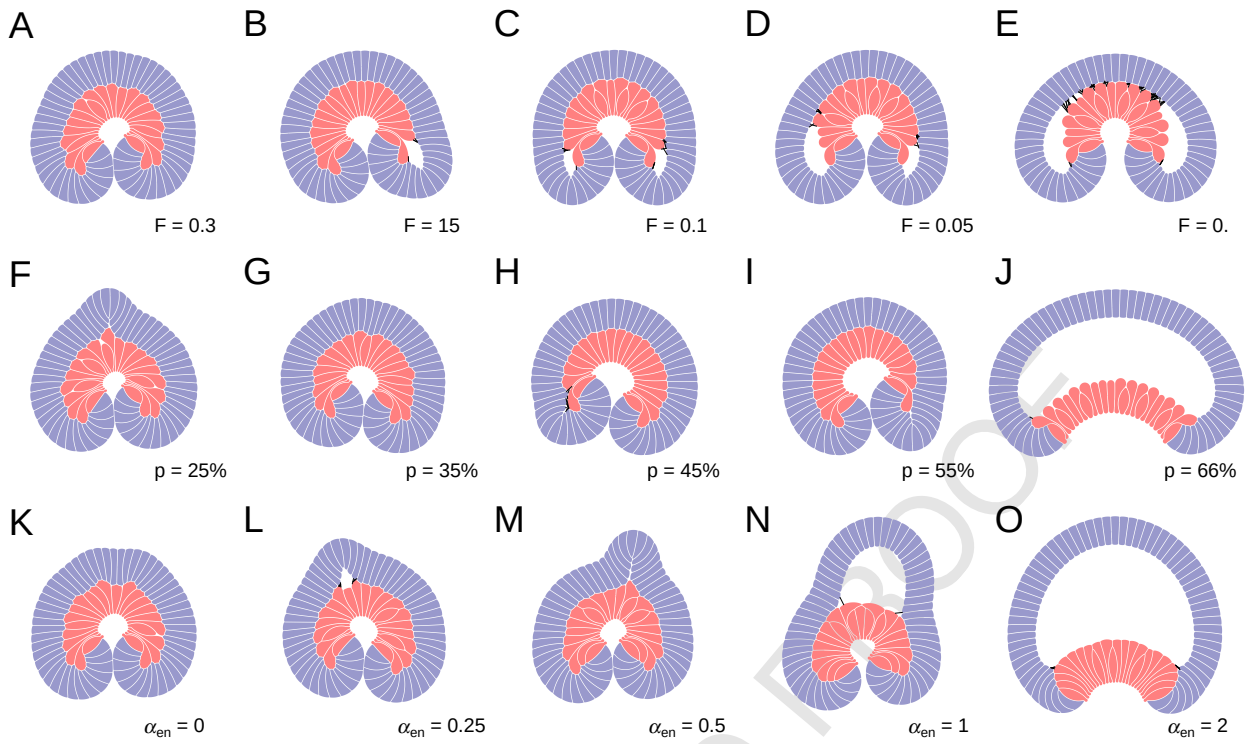

Fig. 8. Simulation parameter variation. In each row a single parameter is varied. The remaining parameters are set to their default values (Table 1). In the first row, the filopodial force (F) is successively reduced resulting in zippering failures; A corresponds to the default parameter value. In the second row apical constriction (p) is successively reduced; G corresponds to the default parameter value. In the third row endodermal cell–cell adhesion (α_{en-en}) is successively increased; *K* corresponds to the default parameter value.

which pushes their neighbors' apico-lateral sides. Any cell that is caught between two such squatting cells is effectively "pinched" causing it to expand basally and bulge over its squatting neighbors.

From this perspective, we find that bottle cells are likely a natural consequence of the mechanics of the system and a specific regulatory program for actively shaping the cells is not required. Although all the mechanical properties of the system are certainly genetically encoded, we find that bottle cells emerge from the general mechanical context of the endodermal domain, rather than each columnar cell being molded into a bottle cell by a genetic program that operates on the cytoskeleton, forming an apical bottleneck and bulging basal end. Therefore, we believe that bottle cells are indirect consequences of genetic regulation and are not explicitly defined genetically. This echoes Hardin and Keller's (1988) work on *Xenopus* bottle cells. In their study, Hardin and Keller found that the bottle cells of the vegetal involuting marginal zone (IMZ) were a product of a combination of (a) individual cell shape changes and (b) the particular mechanical and geometric context of the surrounding tissues. We agree with their assessment and add that individual cell shape changes, i.e. apical constriction, are only necessary to induce bottle cells to the extent that they increase apico-basal contractility.

In terms of direct genetic regulation, we propose that the necessary ingredients for bottle cell formation are: (a) strong apico-basal contractility (in response to apico-basal strain, for example) and (b) reduced cell–cell adhesion. Additionally, the cells must also be laterally constrained. Hardin and Keller (1988) observed that the stiffness of neighboring tissue contributes to bottle cell formation. Following their experiments, if we simulate an explant of the blastula in which the lateral most cells are not subject to pressure from their neighbors and can move more freely, we find that the cells become bottle shaped only transiently, as the explant curls to allow the cells to contract (Movie 3). The whole mechanical and geometric context of the cells must therefore be taken into account, Why do some cells contract, forming squat cells, while others do not, forming bottle cells? We do not think that this is the result of biological differentiation between squat and bottle cells. Rather, this phenomenon can be explained as a global energy minimization of the endoderm under high contractility/low cell–cell adhesion conditions.

Viscous mechanical systems move such that their potential energy is minimized. In the case of the *Nematostella* endoderm, we found that the peculiar organization of this domain emerges from this principle (Fig. 9A). Comparing the total elastic potential energy of the bottle cell configuration and the columnar configuration we found that the total cortex energy for the latter was 13% lower (Fig. 9B), even though the bottle cells are more elongated than their columnar counterparts (Fig. 9C, Movie 2). This is because the squat cells contract substantially more than the bottle cells elongate, resulting in a net decrease of the potential energy of the system.

Our view is that there may be a "continuum" of epithelial organization equilibrium states in which at one end there is the regular epithelial columnar organization and at the opposite end the alternating squat/bottle configuration. The organization state depends on the relative strength of cell contractility versus cell–cell adhesion. Columnar organizations are dominated by cell–cell adhesion, whereas in the bottle cell configuration cell contractility would be the dominant force. From this perspective, one can understand the morphological differences between systems as a variation of this force balance. In the model we eliminate cell–cell adhesion within the endoderm completely, and so we obtain a very pronounced bottle/squat configuration. *In vivo*, however, cell–cell adhesion is not completely absent and so the bottle cell configuration is not as extreme as in the model. If one could gradually increase cell–cell adhesion in the endoderm during *Nematostella* invagination, we would expect the domain to take on less extreme configurations with increasing adhesiveness (as seen in the model). Conversely, if one could down-regulate cell–cell and cell–ECM adhesion during, say,

Please cite this article as: Tamulonis, C., et al., A cell-based model of *Nematostella vectensis* gastrulation including bottle cell formation, invagination and zippering, Dev. Biol. (2010), doi:10.1016/j.ydbio.2010.10.017

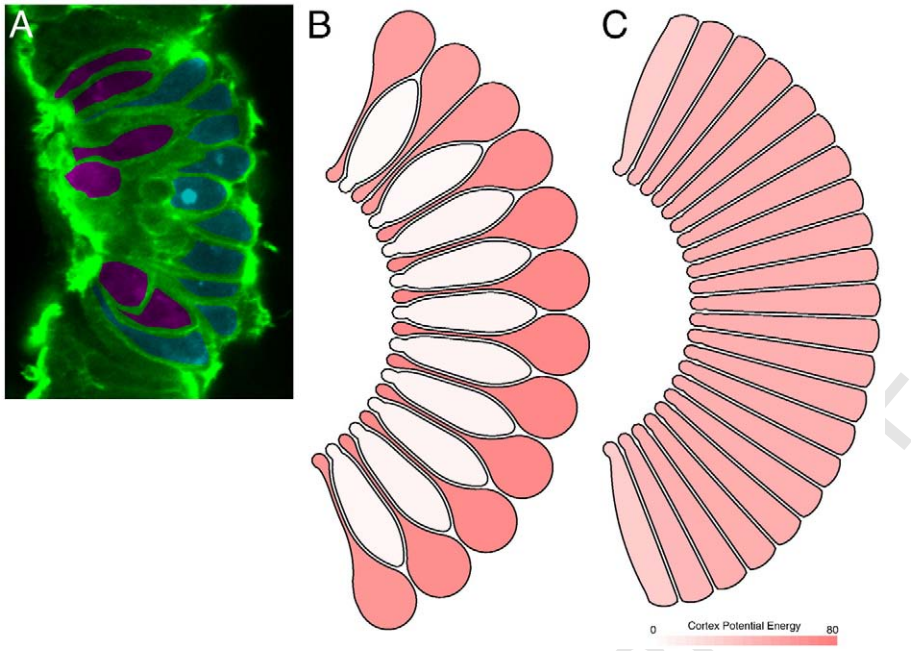

Fig. 9. Bottle cell formation. (A) Close-up of an endodermal plate during invagination showing both bottle (e.g. cells highlighted in red) and squat cells (blue) (B, C) Two different configurations of the model endoderm. (B) Endodermal cells are only bound apically. During apical constriction the domain assumes a bottle cell configuration. (C) Cells are bound apically and basally, forcing the cells to remain columnar during apical constriction. Total potential energy of the cell cortices in (B) is 13% lower compared to (C).

Drosophila ventral furrow formation, we would expect the domain to go from perfectly columnar to a bottle cell configuration.

Finally, bottle/squat cells probably do not have a specific function that depends on their shape. They seem to be just a side effect of high cell strain and low cell–cell adhesion. These two characteristics do have a function though, as we explore in the model. The high strain produces invagination whereas the reduced cell–cell adhesion allows the endoderm to spread over the basal ectoderm. From this viewpoint statement such as "Bottle cells are required for the initiation of primary invagination in the sea urchin embryo" (Kimberly and Hardin, 1998) may be somewhat misleading. As we see it, during invagination the bottle cells have no function which relies on their shape and it is most likely the apical–basal strain caused by apical constriction that actually drives invagination, with bottle cell formation being a mere side effect.

The model qualitatively explains the morphometric features of gastrulation

We find that the gastrulation simulations qualitatively capture many morphometric features of *Nematostella* gastrulation (sup. Fig. 3). In the embryos measured, we found that the thickness of the endoderm increased sharply at the onset of gastrulation, followed by a gradually thinning, whereas the ectoderm appears to thin somewhat followed by a gradual increase in thickness. This is observed during simulations as well. The sharp increase in the endoderm thickness can be attributed to apical constriction, which forces the cells to elongate. The cells gradually retract to their normal height as tension is released during invagination. As they do so, they also expand laterally and consequently the endoderm fans out into the blastocoel, causing its basal surface to expand and allowing the cells to contract more due to the extra space. The tighter the apical constriction, the more the endoderm will fan out and the larger the basal endoderm surface will become. This expansion of the basal surface is necessary, as initially the basal surface of the endoderm is far smaller than that of the ectoderm, although by the end of gastrulation the two must match.

Although the model captures the principal features *Nematostella* gastrulation well, it is lacking in some secondary features. For example, in real embryos the ectoderm is not homogenously thick, but differentially thick along the oral/aboral axis, being thickest closer to the oral pole of the embryo and thinner at the aboral pole (Fig. 4F). This may in part be explained by artifacts related to 2D modeling (see below), but is also almost certainly related to the simplicity of the model in terms of both the processes included and how the included processes were modeled. The model can be improved by refining its existing components, e.g. using a more sophisticated viscoelastic cellular cortex model, and well as adding new ones (see below). We believe, however, that the model as presented is an improvement on previous cell-based models.

Apico-basal contraction of the endoderm

In the embryo, after an initial thickening the endoderm continuously contracts its apico-basal length eventually becoming thinner than it was initially. Beyond the zippering phase of gastrulation, the endoderm has been observed to continue to thin as the pharyngeal ectoderm involutes (Magie et al., 2007). The ectoderm thickness seems to be complementary to that of the endoderm, initially thinning, then thickening as zippering progresses and finally becoming thicker than its initial state and thicker than the endoderm. In the model, the ectoderm thins due to cell contractility and is later pulled back to its initial height through zippering, while the endoderm thickens due to apical constriction and gradually relaxes to its original height. Thus at the end of the simulation, the endoderm and ectoderm have the same height, and the endoderm does not thin to the extent seen in the real embryo. It is plausible that the endoderm in the real system actively contracts apico-basally during gastrulation, and that continued contraction after zippering is completed may cause, or simply allow, the pharyngeal ectoderm to involute. In the model, increasing the contractility in the endoderm after zippering completes not only causes the endoderm to thin but also to curl at the ecto/endoderm boundary, causing the ectoderm to involute.

Please cite this article as: Tamulonis, C., et al., A cell-based model of *Nematostella vectensis* gastrulation including bottle cell formation, invagination and zippering, Dev. Biol. (2010), doi:10.1016/j.ydbio.2010.10.017

Volume regulation

Does the blastocoel play a role during *Nematostella* gastrulation? Magie et al. (2007) noted that aboral ectoderm clones marked with dextran deposited some dextran into the blastocoel during gastrulation, which was later taken up by endodermal cells. Lateral ectodermal and endodermal clones did not exhibit this behavior. Complementing these experiments, we injected dextran into the blastocoel of late-blastula embryos. We found that all cells took up dextran, but that the endodermal cells took up more per cell compared to the ectoderm ($N = 3$, sup. Fig. S2). The two experiments suggest that there is a net flux of material from the aboral ectoderm into the blastocoel and that the there is a net influx of blastocoel material into the endoderm. The morphometric statistics we performed indicate that the endoderm nearly doubles in volume during gastrulation, which is consistent with this view. We were unable to detect a corresponding drop in the ectoderm volume, however, although at the beginning of gastrulation the ectoderm does thin substantially, especially at the aboral pole. This is probably because the ectoderm loses only a small fraction of its volume, and since the ectoderm volume variance is large, the difference would be difficult to detect.

It is also possible that the ecto/endoderm boundary is not static and that the endoderm grows by recruiting adjoining ectodermal cells as gastrulation proceeds. Although the endoderm breadth does indeed increase, the ectoderm breadth does not change significantly indicating that the endoderm probably does not grow at the expense of the ectoderm. Instead, the increasing volume and decreasing thickness of the endoderm can account for the increase in the endoderm breadth. Marking experiments to track the ecto/endoderm boundary could help to definitively resolve this issue.

2D versus 3D models

Nematostella embryos do not remain perfectly radially symmetric during gastrulation. The blastopore can assume many irregular shapes, such as slit-like or polygonal configurations, but is rarely disk shaped. So far no evidence has been found that gastrulation is an asymmetric process (although asymmetric gene expression around the oral/aboral axis does occur) or that the asymmetry is somehow essential to the final result. We have therefore assumed that we can model *Nematostella* gastrulation based on a 2D cross section of the embryo.

One important aspect that is not captured by this 2D model is hoop stress. Hoop stress provides support to radially symmetric structures, such as the *Nematostella* blastula. Imagine the embryo as a series of hoops centered on the oral–aboral axis of the blastula. The equatorial hoop, placed halfway between the poles has the full diameter of the embryo but towards the poles the hoops decrease in diameter tending towards zero. The sequence thus resembles the latitudinal lines of a globe. Each hoop is composed of an elastic material that resists any change in the hoop's length. Therefore, any radial stress (i.e. perpendicular to the primary axis) applied to the hoops would be resisted. Both apical constriction and zippering by filopodia are two examples of radial stress that act to pull the blastoderm towards the primary axis. In a 3D model, hoop stress would provide resistance to these processes and would probably keep the embryo stretched laterally during gastrulation, unlike what is seen in the later stages of the simulation during which the embryo diameter contracts excessively while extending in length along the primary axis.

Outlook

Our simulations suggest that the coeloblastula requires a reinforced apical surface to maintain its proper dimensions, which would otherwise be larger, if cell contractility is the dominant force, or smaller, if cell–cell adhesion dominates. Experiments that alter apical stiffness, cell contractility and/or cell–cell adhesion in blastulae could confirm our observations.

The model also suggests several experiments that may give new insights into bottle cell formation. We predict that in any epithelial system in which the cells are under considerable apical–basal strain (due to apical constriction for example) an accompanying down-regulation of cell–cell adhesion will induce bottle cell formation. Conversely, bottle cell formation can be inhibiting by relaxing cell strain, down-regulating contractility and/or up-regulating cell–cell adhesion.

Finally, as more functional experiments with *Nematostella* gastrulation are performed, modeling and morphometrics could be useful tools to distinguish subtle differences between mutants and wild-type. Modeling can also help to explain why and how gastrulation will fail when a particular process is disabled and conversely will help to identify which processes were affected in a given mutant.

Supplementary materials related to this article can be found online at doi:10.1016/j.ydbio.2010.10.017.

Acknowledgments

Special thanks to Mark Martindale and the Kewalo Marine Laboratory, Hawaii, USA.

CT is funded by the Fundação para a Ciência e Tecnologia (FCT), Portugal. MP and JK are funded by EU MORPHEX Project (contract #043322 NEST).

References

Byrum, C.A., Martindale, M.Q., 2004. Gastrulation in the Cnidaria and the Ctenophora. Gastrulation: From Cells to Embryo.

Chauhan, B.K., Disanza, A., Choi, S.-Y., Faber, S.C., Lou, M., Beggs, H.E., Scita, G., Zheng, Y., Lang, R.A., 2009. Cdc42- and IRSp53-dependent contractile filopodia tether presumptive lens and retina to coordinate epithelial invagination. Development 136, 3657–3667.

Chen, H.H., Brodland, G.W., 2000. Cell-level finite element studies of viscous cells in planar aggregates. J. Biomech. Eng. 122, 394–401.

Darling, J.A., Reitzel, A.R., Burton, P.M., Mazza, M.E., Ryan, J.F., Sullivan, J.C., Finnerty, J.R., 2005. Rising starlet: the starlet sea anemone, Nematostella vectensis. Bioessays 27, 211–221.

Davidson, L.A., Joshi, S.D., Kim, H.Y., Dassow, M.v., Zhang, L., Zhou, J., 2010. Emergent morphogenesis: elastic mechanics of a self-deforming tissue. J. Biomech. 43, 63–70.

Davidson, L.A., Koehl, M.A., Keller, R., Oster, G.F., 1995. How do sea urchins invaginate? Using biomechanics to distinguish between mechanisms of primary invagination. Development 121, 2005–2018.

Davidson, L.A., Oster, G.F., Keller, R.E., Koehl, M.A., 1999. Measurements of mechanical properties of the blastula wall reveal which hypothesized mechanisms of primary invagination are physically plausible in the sea urchin Strongylocentrotus purpuratus. Dev. Biol. 209, 221–238.

Drasdo, D., Höhme, S., 2005. A single-cell-based model of tumor growth in vitro: monolayers and spheroids. Phys. Biol. 2, 133–147.

Fritzenwanker, J.H., Genikhovich, G., Kraus, Y., Technau, U., 2007. Early development and axis specification in the sea anemone Nematostella vectensis. Dev. Biol. 310, 264–279.

Garnett, H.M., 1980. A scanning electron microscope study of the sequential changes in morphology occuring in human fibroblasts placed in suspension culture. Cytobios 27, 7–18.

Graner, F., Glazier, J., 1992. Simulation of biological cell sorting using a two-dimensional extended Potts model. Phys. Rev. Let. 69, 2013–2016.

Hardin, J., Keller, R., 1988. The behaviour and function of bottle cells during gastrulation of Xenopus laevis. Development 103, 211–230.

Honda, H., Motosugi, N., Nagai, T., Tanemura, M., Hiiragi, T., 2008. Computer simulation of emerging asymmetry in the mouse blastocyst. Development 135, 1407–1414.

Jacinto, A., Wood, W., Balayo, T., Turmaine, M., Martinez-Arias, A., Martin, P., 2000. Dynamic actin-based epithelial adhesion and cell matching during Drosophila dorsal closure. Curr. Biol. 10, 1420–1426.

Keller, R., Davidson, L.A., Shook, D.R., 2003. How we are shaped: the biomechanics of gastrulation. Differentiation 71, 171–205.

Kimberly, E.L., Hardin, J., 1998. Bottle cells are required for the initiation of primary invagination in the sea urchin embryo. Dev. Biol. 204, 235–250.

Kraus, Y., Technau, U., 2006. Gastrulation in the sea anemone Nematostella vectensis occurs by invagination and immigration: an ultrastructural study. Dev. Genes Evol. 216, 119–132.

Lecuit, T., Lenne, P.-F., 2007. Cell surface mechanics and the control of cell shape, tissue patterns and morphogenesis. Nat. Rev. Mol. Cell Biol. 8, 633–644.

Please cite this article as: Tamulonis, C., et al., A cell-based model of *Nematostella vectensis* gastrulation including bottle cell formation, invagination and zippering, Dev. Biol. (2010), doi:10.1016/j.ydbio.2010.10.017

Magie, C.R., Daly, M., Martindale, M.Q., 2007. Gastrulation in the cnidarian Nematostella vectensis occurs via invagination not ingression. Dev. Biol. 305, 483–497.
Marée, A.F., Hogeweg, P., 2001. How amoeboids self-organize into a fruiting body: multicellular coordination in Dictyostelium discoideum. Proc. Natl Acad. Sci. USA 98, 3879–3883.
Marlow, H.Q., Martindale, M.Q., 2007. Embryonic development in two species of scleractinian coral embryos: symbiodinium localization and mode of gastrulation. Evol. Dev. 9, 355–367.
Martin, A., Kaschube, M., Wieschaus, E., 2008. Pulsed contractions of an actin–myosin network drive apical constriction. Nature 457, 495–499.
Martin, P., Parkhurst, S.M., 2004. Parallels between tissue repair and embryo morphogenesis. Development 131, 3021–3034.
Odell, G., Alberts, J., Munro, E., Littlefield, R., 2004. In silico cytoskeletal dynamics. Mol. Biol. Cell 15, 236A–A.
Odell, G.M., Oster, G., Alberch, P., Burnside, B., 1981. The mechanical basis of morphogenesis: I. Epithelial folding and invagination. Dev. Biol. 85, 446–462.
Palsson, E., Othmer, H.G., 2000. A model for individual and collective cell movement in Dictyostelium discoideum. Proc. Natl Acad. Sci. USA 97, 10448–10453.
Pouille, P.-A., Farge, E., 2008. Hydrodynamic simulation of multicellular embryo invagination. Phys. Biol. 5, 15005.
Putnam, N.H., Srivastava, M., Hellsten, U., Dirks, B., Chapman, J., Salamov, A., Terry, A., Shapiro, H., Lindquist, E., Kapitonov, V.V., Jurka, J., Genikhovich, G., Grigoriev, I.V., Lucas, S.M., Steele, R.E., Finnerty, J.R., Technau, U., Martindale, M.Q., Rokhsar, D.S., 2007. Sea anemone genome reveals ancestral eumetazoan gene repertoire and genomic organization. Science 317, 86–94.
Rauzi, M., Verant, P., Lecuit, T., Lenne, P.-F., 2008. Nature and anisotropy of cortical forces orienting Drosophila tissue morphogenesis. Nat. Cell Biol. 10, 1401–1410.
Shook, D., Keller, R., 2003. Mechanisms, mechanics and function of epithelial–mesenchymal transitions in early development. Mech. Dev. 120, 1351–1383.
Vasioukhin, V., Bauer, C., Yin, M., Fuchs, E., 2000. Directed actin polymerization is the driving force for epithelial cell–cell adhesion. Cell 100, 209–219.
Weliky, M., Oster, G., 1990. The mechanical basis of cell rearrangement: I. Epithelial morphogenesis during Fundulus epiboly. Development 109, 373–386.

Please cite this article as: Tamulonis, C., et al., A cell-based model of *Nematostella vectensis* gastrulation including bottle cell formation, invagination and zippering, Dev. Biol. (2010), doi:10.1016/j.ydbio.2010.10.017